IEEE Access
Multidisciplinary | Rapid Review | Open Access Journal

Received February 26, 2021, accepted March 29, 2021, date of publication March 31, 2021, date of current version April 9, 2021.

Digital Object Identifier 10.1109/ACCESS.2021.3070275

Orientation-Assisted Beam Management for Beyond 5G Systems

ANUM ALI, (Member, IEEE), JIANHUA MO, (Member, IEEE), BOON LOONG NG, (Member, IEEE), VUTHA VA, (Member, IEEE), AND JIANZHONG CHARLIE ZHANG, (Fellow, IEEE)

Standards and Mobility Innovation Laboratory, Samsung Research America, Plano, TX 75023, USA

Corresponding author: Anum Ali (anum.ali@samsung.com)

ABSTRACT Finding the optimal transmit and receive beam pair for reliable communication can be challenging, especially in highly dynamic environments. Side-information from on-board sensors at the user equipment (UE) can be used to aid the beam management (BM) process. In this work, we use the orientation information coming from inertial measurement unit (IMU) for effective BM. Specifically, we use particle filter (PF) to fuse the reference signal received power (RSRP) information with orientation information. We perform extensive simulations using realistic ray-tracing channels, practical beam patterns, and various UE movement and rotation speeds. Simulation results show the proposed strategy can greatly improve the beam prediction accuracy and reduce the power loss caused by sub-optimal beam-selection.

INDEX TERMS Beam management, sensor-aided communication, IMU, particle filter, beyond 5G, 6G.

I. INTRODUCTION

Communication at millimeter wave (mmWave) and terahertz (THz) frequencies is suitable for high data-rate applications owing to large bandwidth available [1]–[3]. The high free-space path loss at these frequencies implies the use of a large antenna array with beamforming at the transmitter and receiver to achieve a sufficient link margin. beam management (BM) is the process of finding and maintaining a suitable beam pair for communication [4]. BM is challenging, particularly for highly mobile scenarios where the channel changes frequently.

In this work, we use the onboard sensor information as a side-information for effective BM at the UE. Specifically, we use the orientation information coming from IMU in addition to RSRP information for BM. The orientation information is readily available as IMUs are part of several consumer electronics including mobile phones, augmented reality (AR)/virtual reality (VR) gadgets, and unmanned aerial vehicles (UAVs) etc.

A. CONTRIBUTIONS

The main contributions of this paper are as follows:

- We fuse the RSRP information and orientation information for effective BM at the UE.
- We formulate the orientation-assisted BM problem as an angle-of-arrival (AoA) tracking problem. The proposed problem formulation respects the hardware constraints of practical mmWave systems and works with arbitrary antenna array geometry and beam codebook. Also, the proposed formulation is valid for the indoor/outdoor scenarios and line-of-sight (LOS)/non-line-of-sight (NLOS) channels. Finally, the proposed formulation is compatible with 5G new radio (NR) signaling and as such the use of the proposed methods does not require any modification to the standard.
- We use PF for information fusion, which ensures that we do not need to assume any explicit model on the evolution of channel path gain. While PF is a well known algorithm, we fill in several gaps to use the PF in our problem. Specifically, we define a particle to include (i) AoA in Cartesian coordinates, and (ii) a gain term including transmit power, channel path gain, and base station (BS) beam gain. We outline strategies to initialize the angles and gains of particles, as well as strategies to update the particles when RSRP information update rate is lower than the orientation information update rate. We also outline a strategy to predict the beams from the particles, and a strategy to predict narrow beams (NBs) from wide beam (WB) measurements.
- We provide simulation results with realistic ray-tracing based multipath channels, practical UE and BS beam

The associate editor coordinating the review of this manuscript and approving it for publication was Ki-Hong Park.

codebooks, and various UE movement and rotation speeds. Evaluation of the proposed strategy in a realistic setup lends credibility to the results.
- The proposed strategy is shown to improve the beam prediction accuracy by up to 15.5% and mean RSRP by up to 3.84 dB when the UE has fast rotation speed.

B. PRIOR WORK

Several sources of side-information have been used to improve BM at mmWave frequencies. Specifically, position of the mobile device/vehicle [5], [6], spatial information extracted from sub-6 GHz channels [7], [8], light detection and ranging (lidar) [9], radar [10], [11], camera [12], [13], hand grip [14] and 3D scene information [15], [16] have been used to reduce the beam-training overhead and/or improve the beam prediction accuracy. This article differs from [5]–[16] in the source of side-information, as we use orientation information coming from IMU at the UE. Note that orientation information is available at the UE and there is no additional signaling overhead needed to use it.

There is some prior work on using orientation information for BM [17]–[20]. In [17], the best beam after orientation change is predicted given the best beam before orientation change and the amount of orientation change. Specifically, the AoA is determined from the best beam. The change in orientation is translated into a change in AoA to predict the best beam after orientation change. In [18], orientation and location of the UE relative to the BS are tracked and are used for beam steering. In [19], the change in pitch is used to track the LOS path between two vehicles. In [20], orientation and location are used in a machine learning (ML) based inverse fingerprinting method for BM.

There are several limitations of the prior work on using orientation information for BM. Specifically, the strategy of [17] will succeed only if the AoA aligns with the peak direction of the best beam, which is not guaranteed. Therefore, any prediction based on erroneous AoA is likely to be sub-optimal. The strategy of [18], i.e., relative position/orientation tracking is useful only in LOS. Further, the beam steering ignores the hardware constraints of practical mmWave devices. The strategy of [19] is useful only in vehicular communication, where the leading and following vehicles have a strong LOS path and change in pitch is the primary source of change in the LOS path. The ML based inverse fingerprinting strategy of [20] requires data collection and training phase, which could be too costly and not scalable, especially to outdoor cellular mobile communications. Finally, the strategies in [17]–[20] do not consider the 5G NR signaling and practical beam codebooks as we do in this work.

Another line of prior work uses AoA tracking to do BM e.g., [21], [22]. This line of work is similar to our work in that we also formulate our problem as an AoA tracking problem. The prior work [21], [22], however, does not use the side-information from IMU as we do. Further, a first-order Gauss-Markov model for the evolution of channel path gain and a Gaussian random walk for the evolution of AoA and angle-of-departure (AoD) is assumed. Assuming explicit models for channel path gain and AoA/AoD make [21], [22] applicable only to limited scenarios. This work does not assume any explicit model for AoA/AoD and path gain evolution.

The rest of this paper is organized as follows: In Section II, we discuss the communication system model. We then formulate the orientation-assisted BM problem in Section III. In Section IV, we outline the details of the proposed PF based orientation-assisted BM strategy. In Section V, we provide numerical results to show the benefit of the proposed strategy. Finally, we conclude the paper in Section VI and outline directions for future work.

Notation: We use the following notation throughout the paper. Bold lowercase $\mathbf{x}$ is used for column vectors, bold uppercase $\mathbf{X}$ is used for matrices, non-bold letters x, X are used for scalers. The j-th entry of a column vector $\mathbf{x}$ is $[\mathbf{x}]_j$. Superscript T and $*$ represent the transpose and conjugate transpose respectively. The $N \times N$ identity matrix is represented by $\mathbf{I}_N$, and the $N \times 1$ zero vector is $\mathbf{0}_{N\times 1}$. A Gaussian random vector with mean $\mathbf{x}$ and covariance $\mathbf{X}$ is $\mathcal{N}(\mathbf{x}, \mathbf{X})$. A Uniform random variable with support $[a, b]$ is $\mathcal{U}[a, b]$. We use $\mathbb{E}[\cdot]$ to denote expectation, and $\bmod(\cdot)$ is the modulo operator. We define functions to convert powers from linear to logarithmic scale and back, i.e., $\text{pow2db}(x) = 10\log_{10}(x)$ and $\text{db2pow}(x) = 10^{\frac{x}{10}}$.

II. SYSTEM MODEL

We consider a communication system shown in Fig. 1 where the RSRP information, as well as orientation information, is used at the UE side for beam prediction.

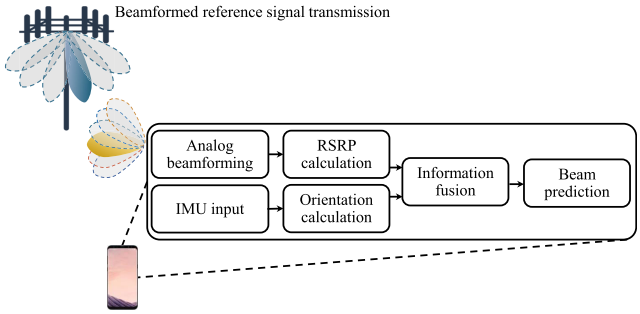

FIGURE 1. The block diagram of a BS-UE communication system in which the UE uses RSRP information as well as orientation information for beam prediction.

A. RSRP INFORMATION

We assume multiple antennas at the BS and UE. In this work, we focus on the downlink (DL) BM, though the proposed strategies can be extended for uplink (UL) operation also. For BM in 5G NR, the BS sends beamformed reference signals (RSs), i.e., synchronization signal blocks (SSBs) and/or channel state information reference signals (CSI-RSs). The UE measures the transmitted RSs using different receive beams, and reports the index and quality of the best transmit beams

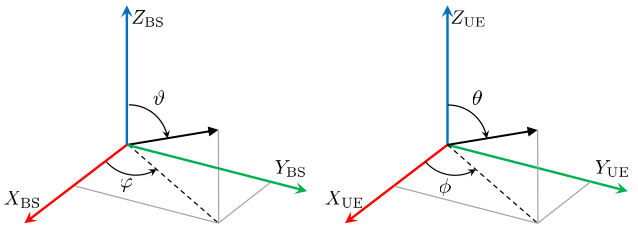

(a) BS local coordinate system. (b) UE local coordinate system.

FIGURE 2. Local coordinate systems of the BS and UE.

to the BS. Based on the UE feedback, the BS decides the best transmit beam for future communication. For simplicity of exposition, we assume only SSB based DL BM.

For BM, the transmit RSs have the power P_{T} dBm. The weights of the transmit beam are selected from a beam codebook containing M_{BS} codewords. A codeword is a set of analog phase-shift (and possibly amplitude scaling) values that are applied to the antenna elements to form a beam. The transmit beam gain is parameterized by azimuth angle φ and zenith angle ϑ shown in Fig. 2a. Specifically, if we use transmit beam $i \in 1, \cdots, M_{\text{BS}}$, then the transmit beam gain in direction (φ, ϑ) is $F_i(\varphi, \vartheta)$ dB. Similarly, the weights of the receive beam are selected from a codebook containing M_{UE} codewords. The receive beam gain is parameterized by azimuth angle ϕ and zenith angle θ shown in Fig. 2b. Specifically, if we use receive beam $j \in 1, \cdots, M_{\text{UE}}$, then the receive beam gain in direction (ϕ, θ) is $G_j(\phi, \theta)$ dB. Note that in our model, the AoD (φ, ϑ) and AoA (ϕ, θ) are in the local coordinates of the BS and UE respectively as shown in Fig. 2.

We assume that SSBs are transmitted with periodicity T_{SS}. Let the time variable t denote the index of the SSB. Then, consider a multipath channel with C paths, such that the path gain of the c-th path at time t is $p_t^{(c)}$ dB, the AoD in the BS local coordinates is $(\varphi_t^{(c)}, \vartheta_t^{(c)})$ and the AoA in the UE local coordinates is $(\phi_t^{(c)}, \theta_t^{(c)})$. If the transmit beam index at time t is i_t and the receive beam index is j_t, then the RSRP s_t corrupted by noise n_t is

$$s_t = P_{\text{T}} + \text{pow2db}\Big(\sum_{c=1}^{C} \text{db2pow}\big(p_t^{(c)} + F_{i_t}(\varphi_t^{(c)}, \vartheta_t^{(c)}) + G_{j_t}(\phi_t^{(c)}, \theta_t^{(c)})\big)\Big) + n_t. \tag{1}$$

In this work, we are interested in the use of UE orientation for BM. Therefore, for simplicity, we assume genie-aided knowledge of the best transmit beam, i.e., $i^\star$ and focus on finding $j^\star$. A conventional BM strategy based only on RSRP information operates in the following manner. With known $i^\star$, the UE maintains an RSRP table $\mathbf{s} \in \mathbb{R}^{M_{\text{UE}} \times 1}$ with all entries initialized to $-\infty$. The UE receives the beamformed SSB by varying the receive beams in a round-robin manner. Specifically, $j_t = \text{mod}(t, M_{\text{UE}}) + 1 \in \{1, \cdots, M_{\text{UE}}\}$. This way, the j_t-th entry of the RSRP table can be set as

$$[\mathbf{s}]_{j_t} = s_t, \tag{2}$$

and the best receive beam $\hat{j}^\star$ is then found at any given time t as $\hat{j}^\star = \arg\max_j [\mathbf{s}]_j$. Note that, it requires M_{UE} SSB periods to update the whole SSB table, which could render some entries in the table outdated due to temporal changes, e.g., UE orientation change.

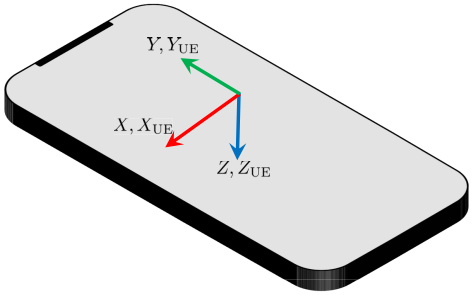

FIGURE 3. The orientation of the phone when the UE local coordinate system $X_{\text{UE}}Y_{\text{UE}}Z_{\text{UE}}$ is aligned with global coordinate system XYZ.

B. ORIENTATION INFORMATION

We intend to use orientation information in addition to RSRP information for BM as shown in Fig. 1. The orientation information comes from an IMU that may include a three-axis gyroscope (for measurement of angular velocity), a three-axis accelerometer (for acceleration measurement), and a three-axis magnetometer (for magnetic field measurement) [23]. We consider the coordinate system shown in Fig. 3 for UE. The global coordinate system is represented using XYZ and the UE local coordinate system is represented using $X_{\text{UE}}Y_{\text{UE}}Z_{\text{UE}}$. In Fig. 3, the global coordinate system and the local coordinate system of the UE are aligned. We assume a rotations around Z, Y, and X axis, in that order [24]. The rotation around Z, Y and X are denoted by α, β, and γ respectively [24]. Let the individual rotation matrices around each axis be $\mathbf{R}_Z(\alpha)$, $\mathbf{R}_Y(\beta)$, and $\mathbf{R}_X(\gamma)$. These matrices are defined as

$$\mathbf{R}_Z(\alpha) = \begin{bmatrix} \cos\alpha & -\sin\alpha & 0 \\ \sin\alpha & \cos\alpha & 0 \\ 0 & 0 & 1 \end{bmatrix}, \tag{3}$$

$$\mathbf{R}_Y(\beta) = \begin{bmatrix} \cos\beta & 0 & \sin\beta \\ 0 & 1 & 0 \\ -\sin\beta & 0 & \cos\beta \end{bmatrix}, \tag{4}$$

and

$$\mathbf{R}_X(\gamma) = \begin{bmatrix} 1 & 0 & 0 \\ 0 & \cos\gamma & -\sin\gamma \\ 0 & \sin\gamma & \cos\gamma \end{bmatrix}. \tag{5}$$

Now, we can construct a composite rotation matrix $\mathbf{R}(\alpha, \beta, \gamma)$ based on individual rotation matrices $\mathbf{R}_Z(\alpha)$, $\mathbf{R}_Y(\beta)$, and $\mathbf{R}_X(\gamma)$, i.e., $\mathbf{R}(\alpha, \beta, \gamma) = \mathbf{R}_Z(\alpha)\mathbf{R}_Y(\beta)\mathbf{R}_X(\gamma)$. The orientation of the mobile phone at time t is determined by α_t, β_t and γ_t. In this work, in order to keep the model simple, we assume that the measurements from IMU are processed

and integrated so that the orientation at time t is determined by $\hat{\alpha}_t$, $\hat{\beta}_t$ and $\hat{\gamma}_t$, which are erroneous estimates of α_t, β_t and γ_t.

III. PROBLEM FORMULATION

To understand how the orientation information can help in BM for the UE, consider a toy example. Assume that the channel between BS and UE is LOS, i.e., there is one strong path. Further, assume that the AoA (in the UE local coordinate system) is perfectly known, which can be used to find the best UE beam. Specifically, if the beam-gains of all the beams are known, it can be determined which beam has the highest gain for the current AoA. The beam with the highest gain for the current AoA is also the best beam for transmission/reception. In such a situation, if the UE orientation changes, the new AoA (and the new best beam) can be found based on the orientation information alone. This simple strategy, though useful to explain the intuition behind the use of orientation information in BM, is not practical. First, accurate AoA estimation is very challenging due to the hardware constraints, i.e., phase-shifter based analog beamforming. Second, the orientation information obtained from sensors is erroneous. Third, the channel experiences changes that cannot be observed through IMU sensors, e.g., multipath fading. Therefore, the orientation information and the RSRP information need to be fused.

To fuse the orientation and RSRP information, we formulate the BM problem as an AoA tracking problem in the UE local coordinate system. This is again assuming that the beam-gains of all beams are known, and once the AoA is determined, the beam that has the best gain for the AoA can be determined. We formulate the problem by assuming a single path channel. The numerical results presented in Section V, however, show that the proposed strategy works well in practical dynamic multipath channels obtained using ray-tracing. Further, the single path assumption is fair in mmWave frequency cellular operation, as the channel has few strong paths. The number of strong paths in the effective channel, including BS beamforming, are further reduced due to a large number of antennas at the BS and the use of high gain narrow beams. If we consider a single path channel in (1), and drop the superscript (c), then the RSRP is

$$s_t = P_{\mathrm{T}} + p_t + F_{i_t}(\varphi_t, \vartheta_t) + G_{j_t}(\phi_t, \theta_t) + n_t. \tag{6}$$

Because the BS beam is transparent to the UE, we can define a gain term

$$g_t = P_{\mathrm{T}} + p_t + F_{i_t}(\varphi_t, \vartheta_t), \tag{7}$$

and simply write the RSRP as

$$s_t = g_t + G_{j_t}(\phi_t, \theta_t) + n_t. \tag{8}$$

Note that, the AoA at time t can be described in polar coordinates, i.e., (ϕ_t, θ_t) as in Fig. 2b and (8). The same AoA can also be described in the Cartesian coordinates using a unit vector in the direction (ϕ_t, θ_t). Specifically, we collect the three components of the Cartesian AoA in a vector $\mathbf{a}_t \in \mathbb{R}^{3\times 1}$ as

$$\mathbf{a}_t = \begin{bmatrix} x_t \\ y_t \\ z_t \end{bmatrix} = \begin{bmatrix} \sin(\theta_t)\cos(\phi_t) \\ \sin(\theta_t)\sin(\phi_t) \\ \cos(\theta_t) \end{bmatrix}. \tag{9}$$

For ease of subsequent exposition, we define a function pol2car$(\cdot)$ for polar to Cartesian coordinates conversion. Using this function, (9) can be written as $\mathbf{a}_t = \text{pol2car}(\phi_t, \theta_t)$. The Cartesian coordinate representation of the angle makes it convenient to describe the evolution of angle due to orientation change. Specifically, let us define orientation at time t via a matrix $\mathbf{R}_t \triangleq \mathbf{R}(\alpha_t, \beta_t, \gamma_t)$, and similarly orientation at time $t-1$ via a matrix $\mathbf{R}_{t-1}$. If the AoA in global coordinates is represented as $\mathbf{a}_{\mathrm{g}}$, then the AoA in UE's local coordinate system at time $t-1$ is

$$\mathbf{a}_{t-1} = \mathbf{R}_{t-1}\mathbf{a}_{\mathrm{g}}, \tag{10}$$

and the AoA in UE's local coordinate system at time t is

$$\mathbf{a}_t = \mathbf{R}_t\mathbf{a}_{\mathrm{g}}. \tag{11}$$

Note that, the rotation has no impact on the global AoA $\mathbf{a}_{\mathrm{g}}$, i.e., it does not change between $t-1$ and t. From (10), we get $\mathbf{R}_{t-1}^{\mathsf{T}}\mathbf{a}_{t-1} = \mathbf{a}_{\mathrm{g}}$, due to the unitary nature of the matrix $\mathbf{R}_{t-1}$. Now, the AoA in UE's local coordinates at time t, i.e., $\mathbf{a}_t$ can be related to the AoA in UE's local coordinates at time $t-1$, i.e., $\mathbf{a}_{t-1}$ as

$$\mathbf{a}_t = \mathbf{R}_t\mathbf{R}_{t-1}^{\mathsf{T}}\mathbf{a}_{t-1}. \tag{12}$$

The relationship (12) does not depend on global AoA $\mathbf{a}_{\mathrm{g}}$. Hence, with no risk of confusion, here onwards we refer to the AoA in UE's local coordinates simply as the AoA or the angle. As polar angles (ϕ_t, θ_t) in (8) are equivalent to Cartesian angles $\mathbf{a}_t$ in (12), we can write (8) equivalently as

$$s_t = g_t + G_{j_t}(\mathbf{a}_t) + n_t. \tag{13}$$

Our objective is to fuse the orientation information, captured through angle evolution in (12), and the RSRP information in (13), to do effective BM.

IV. PF TO FUSE RSRP AND ORIENTATION INFORMATION

The problem of fusing RSRP and orientation information can be solved using PF. The PF is a non-parametric filter that approximates the posterior by finitely many samples called "particles" [25]–[27]. We leave the discussion on our choice of using PF over other nonlinear filters from the Kalman family to a later point in this Section. At this stage, we proceed by laying down the preliminaries of using PF to fuse the RSRP and orientation information.

A. PROPOSED BM STRATEGY

Our formulation of UE BM by fusing RSRP and orientation information is based on Cartesian AoA tracking. Specifically, the evolution model of the AoA is given in (12), which needs

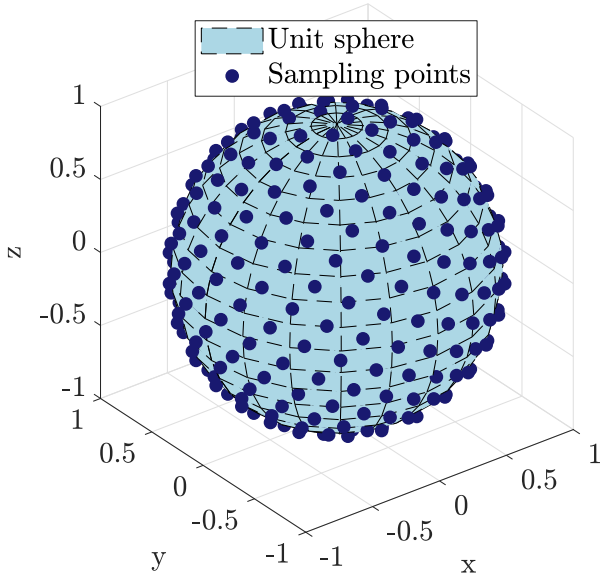

FIGURE 4. Uniform sampling of the unit sphere based on Fibonacci grid with $L = 300$ points.

Algorithm 1 Procedure to Get Uniformly Spaced Particles and Their Gains

Input: L, s_t, G_{j_t}
Initialization: $\mathcal{R}_t = \emptyset$
1: **for** $\ell = 1 : L$ **do**
2: $\theta^{[\ell]} = \cos^{-1}\left(1 - \frac{2(\ell-1)+1}{L}\right)$
3: $\phi^{[\ell]} = 2\pi \mod \left(\frac{2(\ell-1)}{1+\sqrt{5}}, 1\right)$
4: $\mathbf{a}^{[\ell]} = \text{pol2car}(\theta^{[\ell]}, \phi^{[\ell]})$
5: $g_t^{[\ell]} = s_t - G_{j_t}(\mathbf{a}^{[\ell]})$
6: $\mathcal{R}_t = \mathcal{R}_t \cup \{\mathbf{a}_t^{[\ell]}, g_t^{[\ell]}\}$
7: **end for**
Output: return $\mathcal{R}_t$.

to be tracked. For AoA tracking, it is natural that a particle contains the angle. Furthermore, from (13), note that we need to keep track of the gain g_t in order to explain the RSRP in the form of UE beam-gain parameterized by AoA, i.e., $G_{j_t}(\mathbf{a}_t)$. Therefore, we include the gain g_t also in defining a particle. Overall, a particle has two components, one to track angle $\mathbf{a}_t$, given in (12), and one to track gain g_t, given in (7).

We consider that the total number of particles in the filter is M. In the beginning, we need to initialize all the M particles. We define a particle set $\mathcal{P}_t$ that contains the M particles at time t. So initially, we need to obtain $\mathcal{P}_1$. For initializing the angles of the M particles, a good choice is uniform spacing based on Fibonacci grid [28]. We refer to the particles that have uniformly spaced angles simply as uniformly spaced particles. The procedure to obtain uniformly spaced particles and their gains is given in Algorithm 1. The uniformly spaced particles obtained through the procedure of Algorithm 1 are shown in Fig. 4. Note that, uniformly spaced particles based on the Fibonacci grid is only one initialization option and other strategies can be used. If some prior knowledge about the environment is available, it can be used to initialize the particles, e.g., if there is a higher likelihood of having the AoA in certain angular regions, a higher number of particles can be initialized in those regions, and vice versa. Steps 2 to 4 in Algorithm 1 obtain L uniformly spaced polar angles $(\phi^{[\ell]}, \theta^{[\ell]})$ and subsequently obtain Cartesian angles $\mathbf{a}^{[\ell]}$ from polar angles. In the initialization phase, $L = M$ as all particles are uniformly spaced. The gain for the particles is set as in step 5 of Algorithm 1, i.e., by subtracting the receive beam gain from the RSRP s_t. The index j_t is the index of the receive beam used at time t. Note that the sampling strategy used to obtain the angles $\mathbf{a}^{[\ell]}$ has no bearing on the calculation of the gain of a particle $g_t^{[\ell]}$. The calculation of gain in step 5 of Algorithm 1 is based on the relation (13), and the gain $g_t^{[\ell]}$ is calculated given the angle $\mathbf{a}^{[\ell]}$. Therefore the gain calculation is valid for any strategy used for obtaining the angles $\mathbf{a}^{[\ell]}$. For initialization, we use $s_t = s_1$, and $j_t = 1$. Finally, the angles and gains are added to the particle set $\mathcal{R}_t$ in step 6, which is returned as output.

Algorithm 2 The PF Algorithm for Orientation-Assisted BM

Input: $\mathcal{P}_{t-1}, \mathbf{R}_t, \mathbf{R}_{t-1}, G_{j_t}, s_t, \sigma_n^2$
Initialization: $\tilde{\mathcal{P}}_t = \emptyset$
1: **for** $m = 1 : M$ **do**
2: $\mathbf{a}_t^{[m]} = \mathbf{R}_t^{[m]}\left(\mathbf{R}_{t-1}^{[m]}\right)^{\mathsf{T}}\mathbf{a}_{t-1}^{[m]}$
3: $g_t^{[m]} = g_{t-1}^{[m]}$
4: $s_t^{[m]} = g_t^{[m]} + G_{j_t}(\mathbf{a}_t^{[m]})$
5: $w_t^{[m]} = \frac{1}{\sqrt{2\pi\sigma_n^2}} e^{-\frac{(s_t - s_t^{[m]})^2}{2\sigma_n^2}}$
6: $\tilde{\mathcal{P}}_t = \tilde{\mathcal{P}}_t \cup \{\mathbf{a}_t^{[m]}, g_t^{[m]}, w_t^{[m]}\}$
7: **end for**
8: $\mathcal{P}_t = \emptyset$
9: **for** $m = 1 : M - N$ **do**
10: draw i with probability $\propto w_t^{[i]}$
11: $\mathcal{P}_t = \mathcal{P}_t \cup \{\mathbf{a}_t^{[i]}, g_t^{[i]}\}$
12: **end for**
13: Get N uniform particles in $\mathcal{R}_t$ by calling Algorithm 1 with $L = N$, s_t, and G_{j_t}.
14: $\mathcal{P}_t = \mathcal{P}_t \cup \mathcal{R}_t$
Output: return $\mathcal{P}_t$.

We give the PF algorithm tailored for orientation-assisted BM in Algorithm 2. For all the M particles, first, we update the angles of the particles in step 2. We also add randomness to the particles to capture the uncertainty due to erroneous sensor information in step 2. For updating the angles, first, we take out the previous orientation, and then add the new orientation. Specifically, let $\mathbf{a}_{t-1}^{[m]}$ be the angle associated with the particle m at time $t-1$. The process of taking out the old orientation and adding new orientation is accomplished by pre-multiplying the angle $\mathbf{a}_{t-1}^{[m]}$ by $\mathbf{R}_t^{[m]}\left(\mathbf{R}_{t-1}^{[m]}\right)^{\mathsf{T}}$. The matrix $\mathbf{R}_t^{[m]}$ represents the orientation at time t, i.e., the new

orientation, and is defined as

$$\mathbf{R}_t^{[m]} = \mathbf{R}(\hat{\alpha}_t + \tilde{\alpha}_t^{[m]}, \hat{\beta}_t + \tilde{\beta}_t^{[m]}, \hat{\gamma}_t + \tilde{\gamma}_t^{[m]}), \tag{14}$$

where $\tilde{\alpha}_t^{[m]}, \tilde{\beta}_t^{[m]}, \tilde{\gamma}_t^{[m]}$ is the random perturbation generated for the particle m. The random perturbation is generated according to the known sensor error statistics $\sigma_\alpha, \sigma_\beta$ and σ_γ. The matrix $\mathbf{R}_{t-1}^{[m]}$ is defined similarly. In step 3, we update the gains of the particles. Notice that while updating the gain, we simply use the previous gains, and step 3 is only added for completeness. It is possible to use the previous gains because in each time-step we add N particles that contain gains based on new RSRP information s_t. We will elaborate more on this when we discuss steps 13-14. In step 4, we update the RSRP hypothesis for m-th particle, $s_t^{[m]}$, based on the angle and gain of the particle. In step 5, we calculate the weight of the m-th particle based on the actual RSRP at time t, s_t, and the RSRP hypothesis of m-th particle, $s_t^{[m]}$, assuming Gaussian RSRP noise n_t with variance σ_n^2. We then add the gain of the particle m, $g_t^{[m]}$, angle of the particle m, $\mathbf{a}_t^{[m]}$, and weight of particle m, $w_t^{[m]}$, in the temporary particle set $\bar{\mathcal{P}}_t$.

In steps 8-12, we do importance sampling of the particles in $\bar{\mathcal{P}}_t$. Importance sampling is a probabilistic implementation of the Darwinian idea of the survival of the fittest. It ensures that particles remain close to regions in state space with high posterior probability. Specifically, we draw $M - N$ particles using importance sampling. The remaining N particles in every time-step are uniformly spaced. This strategy solves the well-known particle deprivation problem of the PF. Particle deprivation happens when there are not enough particles near the true state and thus it cannot be tracked [26]. In BM, particle deprivation can happen e.g., when the channel changes substantially, i.e., from LOS to NLOS, or the other way around. Such channel changes can cause dramatic changes in the AoA. Once the particles have converged to a certain AoA, without uniform particles throughout the sphere, the new AoA after channel change cannot be tracked. We add uniform particles in step 13 and 14 by following the strategy outlined in Algorithm 1 to obtain uniformly spaced particles and their gains. Note that the gains of these N particles are based on current RSRP s_t. Thus, in each time-step, a fraction of particles contain the current gain information. Therefore, using the proposed strategy the gain is implicitly tracked. We call the set of N uniformly spaced particles $\mathcal{R}_t$, and add these particles to $\mathcal{P}_t$. The particles set $\mathcal{P}_t$ is then returned.

For BM, the best beam needs to be obtained from the particles. One procedure for obtaining the best beam using particles is given in Algorithm 3. First, we define the concept of a beam decision region. The beam decision region of a beam is the angular region in which the gain of the given beam is higher than any other beam in the codebook. Given the number of codewords M_{UE}, the beam-patterns, the angles of the particles at time t, we count the number of particles that fall within the beam decision region of each beam. Subsequently, the beam that has the highest number of particles within its decision region is declared the best beam.

Algorithm 3 Beam Prediction Based on Particles

Input: $\mathcal{P}_t, G_1, \cdots, G_{M_{\text{UE}}}, M, M_{\text{UE}}$

1: $\mathbf{c} = \mathbf{0}_{M_{\text{UE}} \times 1}$
2: **for** $m = 1 : M$ **do**
3: $\quad i^\star = \arg\max_i G_i(\mathbf{a}_t^{[m]})$
4: $\quad [\mathbf{c}]_{i^\star} = [\mathbf{c}]_{i^\star} + 1$
5: **end for**

Output: return $j^\star = \arg\max_j [\mathbf{c}]_j$.

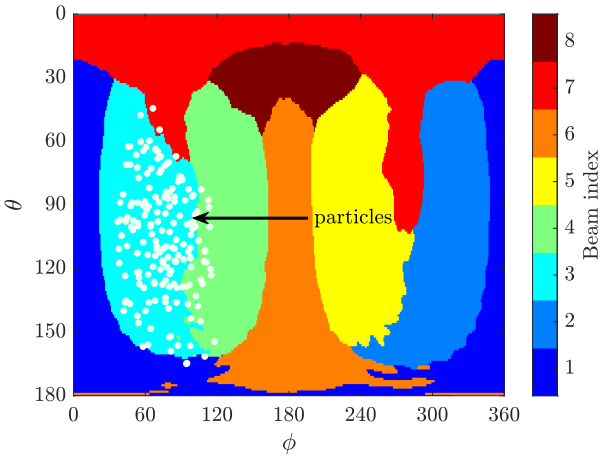

FIGURE 5. Beam decision regions (shown with different colors) of a WB codebook with 8 codewords and particles of the PF. Most of the particles lie in the region where WB 3 has the highest-gain. Therefore, WB 3 is predicted to be the best beam.

One example of this procedure in action is shown in Fig. 5, assuming a WB codebook with 8 codewords. The beam decision regions of different beams are shown with different colors. The beam index corresponding to each color is shown in the colorbar on the right of the figure. The particles are shown in white color. In this example, most of the particles lie in the beam decision region of WB 3, and therefore WB 3 is the predicted best beam. Counting the number of particles can also provide an estimate of the top-n (e.g., top-5) best beams by sorting $\mathbf{c}$ (see Algorithm 3) in descending order and picking the indices of the first n elements. Note that, counting the particles for beam prediction is only one method and other strategies are possible. As an example, it is possible to use the mean of the angles of all particles as an estimate of AoA and then the beam that has the AoA in its beam decision region can be declared the best beam. This method, however, does not readily extend to top-n beam prediction.

B. COMMENTS ON PROPOSED BM STRATEGY

1) REASONS FOR CHOOSING PF

Here we address the reasons for choosing the PF over other nonlinear filters in the Kalman family, e.g., extended Kalman filter (EKF), and unscented Kalman filter (UKF). The RSRP equation, i.e., (13) includes the UE beam-gain in terms of the parameter that we intend to track, i.e., $\mathbf{a}_t$. The beam-pattern, however, is a highly nonlinear function of Cartesian angle $\mathbf{a}_t$.

This is true for even the most trivial beam-patterns that have a closed form, e.g., discrete Fourier transform (DFT) beams. For a high level of non-linearity, it is difficult to guarantee the stability of a filter. High non-linearity also implies that the Gaussian assumption on the posterior typically made in parametric filters including EKF and UKF is not going to strictly hold. Further, the beam-patterns in practice are available only as numerical values determined e.g., by measurements in an anechoic chamber. Therefore, an accurate estimation of the gradient required for EKF becomes difficult. In this case, the derivative can only be approximated, implying approximation error. Another advantage of using PF is that we do not need to explicitly track the gain g_t, as the N uniform particles added in every time-step implicitly include the gain information. The use of EKF or UKF will require explicit tracking of the gain. Explicit tracking will also require a process model for the gain evolution, which can be restrictive/limiting from the practical application point of view.

2) REASON FOR USING CARTESIAN ANGLES

We formulate the angle tracking problem in the Cartesian coordinates. One reason for this choice is that, given the orientation matrices $\mathbf{R}_t$ and $\mathbf{R}_{t-1}$, the relationship between old angle $\mathbf{a}_{t-1}$ and new angle $\mathbf{a}_t$ is linear (see (12)). The alternative possibility was to formulate the problem using polar angles (ϕ, θ). We ruled out a formulation based on polar angles as we observed that erroneous orientation information results in a very high variance in the azimuth angle ϕ. Particularly, note that when the AoA is close to the zenith, a small error can dramatically change ϕ without changing the pointing direction significantly. This artifact implies that polar angle tracking can be difficult.

3) DIFFERENT RSRP AND ORIENTATION INFORMATION RATE

So far we considered RSRP and orientation information rate to be identical. It is, however, possible for RSRP and orientation information rate to be different. From BM point of view, it is more interesting to consider the case when RSRP information has a lower rate compared to orientation information. There are multiple reasons for this. First, if orientation information appears at a slower rate, the proposed strategy will rely heavily on RSRP information, and hence in essence will become similar to the conventional BM that relies only on RSRP information. Second, the IMUs in mobile devices provide information at a rapid rate, e.g., 100 Hz is relatively common [23]. Third, as the orientation information is also used in applications other than BM, concerns other than BM may require that the IMUs be operational at all times. In contrast, reducing the RSRP measurement rate can save power consumption of the device. So far we considered the base rate of both RSRP and orientation information to be $1/T_{\text{SS}}$. We can generalize this by assuming that new RSRP information is available every f SSB periods, i.e., fT_{SS}. As an example, with $f = 1$, we have the case of identical RSRP and orientation information rate, whereas $f = 3$ will mean that RSRP information rate is $3\times$ lower than the orientation information rate.

As for the practicality of having an RSRP information rate lower than orientation information rate, as discussed above, consider the series of articles [29]–[32] in which a measurement-based model for the temporal evolution of the orientation is given. In these articles, a first-order autoregressive model is used for modeling the temporal evolution of the orientation parameters α, β, and γ. The coherence time for the random process is defined as the time in which the autocorrelation function of the random process has decreased to 0.05. This is to say, that the coherence time of the random process used to generate α, β, and γ, is based on the time in which the actual measurements had decorrelated by 95%. The reported measured coherence times for the processes are between 130 ms to 180 ms for the walking users. Based on this observation, it is clear that if 95% decorrelation takes 180 ms, significant change in α, β, and γ can occur in $fT_{\text{SS}} = 60$ ms (i.e., $f = 3$ and $T_{\text{SS}} = 20$ ms).

From the perspective of PF, note that, when the RSRP information rate is lower than orientation information rate, we use the most recent RSRP information in PF. Therefore, s_t represents the most recent RSRP available at time t, and j_t is the index of the beam used for obtaining the most recent RSRP.

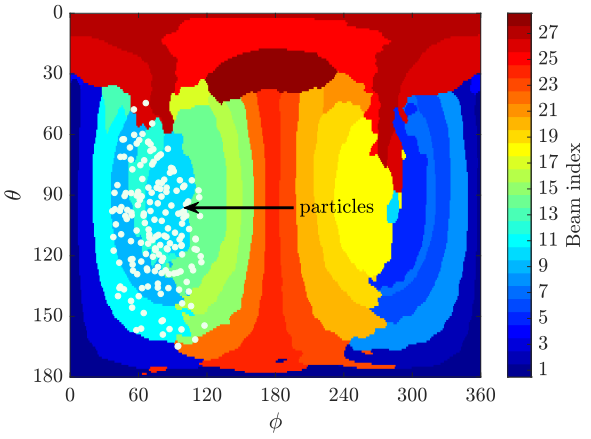

FIGURE 6. Beam decision regions (shown with different colors) of a NB codebook with 28 codewords and particles of the PF. Most of the particles lie in the region where NB 9 has the highest-gain. Therefore, NB 9 is predicted to be the best beam.

4) PREDICTING NBs USING WB RSRPs

Note that the way we decide the best beam is based on counting the number of particles in the beam decision region of a particular beam. This is a particularly interesting approach because it makes it possible to predict the best NB based on RSRPs of the WBs. Specifically, the SSBs are received using the WBs, and the PF as given in Algorithm 2 is run. While counting the number of particles, however, we use the NB decision regions to predict the best NB. To elaborate, we continue with the example of Fig. 5. The particles of Fig. 5 overlaid on the beam decision regions of a NB codebook with 28 codewords are shown in Fig. 6. For the

same set of particles, we use the beam decision regions of NBs to predict the best NB. In this example, the number of particles falling in the beam decision region of NB 9 is the largest, therefore NB 9 is the predicted best beam. The proposed method can be advantageous over receiving SSBs through NBs. This is because WBs are fewer in number, yet they cover the entire angular space, i.e., the whole sphere. Therefore, when the channel state changes, e.g., from LOS to NLOS, the new strong path can be observed quickly, i.e., with fewer SSBs using WBs. Further, the success of PF based BM depends on the concentration of the particles around the AoA of the strong multipath. In our experiments, we have noticed that even with WB operation the particles are quite concentrated and hence can be used reliably for accurate NB prediction.

5) USING PF TO OPTIMIZE UE-OPERATIONS

The state of PF provides information that can help tune other UE-operations. As an example, the concentration of the particles can inform about the channel state. The concentration of particles can be calculated using an angle spread measure, e.g., the measure used in [33], applied to the particles. If the spread is low, i.e., more concentration, the channel state is likely to be LOS, whereas, if the spread is high, i.e., less concentration, the channel state is likely to be NLOS. The knowledge of channel state can in turn be used for other tasks, e.g., to select a codebook optimized for detected channel state. Similarly, if there is a sudden change in the concentration of particles, it can imply a channel state change which can be used as a trigger for certain operations, e.g., in hierarchical beam search, such a trigger can be used to change from beam refinement to full beam search. Finally, the rate at which the weights, calculated in step 5 of Algorithm 2 vary, can suggest the rate of channel change and can be used e.g., to adjust the RSRP information rate, e.g., $f = 1$ when detecting a highly dynamic channel, and $f > 1$ otherwise.

V. SIMULATION RESULTS

We now present the simulation results. We start by discussing the simulation setup in detail in Section V-A. We then show the initial convergence and the ability of PF to avoid particle deprivation when the channel state changes in Section V-B, followed by the supremacy of our proposed strategy compared to conventional BM in Section V-C. We then show that using the proposed strategy NBs can be predicted using WB RSRPs in Section V-D. In Section V-B to V-D, we consider a single antenna BS. Finally, in Section V-E we show the performance of the proposed strategy with a multi-antenna BS.

A. SIMULATION SETUP

1) RAY-TRACING SETUP

We consider the ray-tracing setup shown in Fig. 7. We use Wireless InSite® [34] software for ray-tracing. The considered location is downtown Rosslyn, VA, USA. The color of

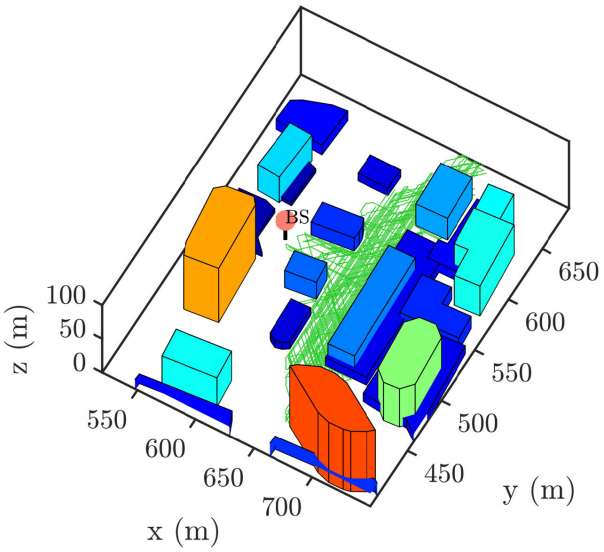

FIGURE 7. The ray-tracing simulation setup of downtown Rosslyn, VA. The location of BS is shown with the salmon color disc, and the UE moves along the trajectory shown by green lines.

the buildings in Fig. 7 corresponds to their height. The total simulation area is 230 m × 295 m × 100 m. All the buildings are made of concrete. The road surface is made of asphalt. The operating frequency is 28 GHz. The location of the BS is shown in Fig. 7 with a salmon color disk with the text BS next to it. The height of the BS is 30 m. The UE moves along a trajectory shown via lines of green color in Fig. 7. The trajectory is generated by the random waypoint model where UE picks a random destination within the cell, moves to the destination with a fixed speed, and again picks another random destination. A* search algorithm is used to find a route from one destination to the next [35]. In the simulation, UE moves through 200 destinations and the total length of the trajectory is around 20 km. Notice that we consider a 120° sector and the UE trajectory is limited by the size of the sector. The number of multipaths at any UE location is $C = 25$.

2) COMMUNICATION SYSTEM PARAMETERS

As we focus on accurate BM for the UE, we consider the BS beam to be known. One simple way to simulate this is to consider a single isotropic antenna at the BS, so the beamforming is not required and $M_{\text{BS}} = 1$. It is worth highlighting that for the BM, a single BS antenna and no beamforming is a pessimistic setup. This is because our AoA tracking based BM formulation assumes that the channel has a single path, so having multipaths only deteriorates the performance of the PF. Practical mmWave or THz BSs will employ a large number of antennas and hence will have high beamforming gain. The high beamforming gain typically implies narrow beams and will sparsify the channel. Hence with BS beamforming, the channel will be more similar to a single path channel. Therefore, the practical multi-antenna BS with high gain beamforming is more favorable for the proposed

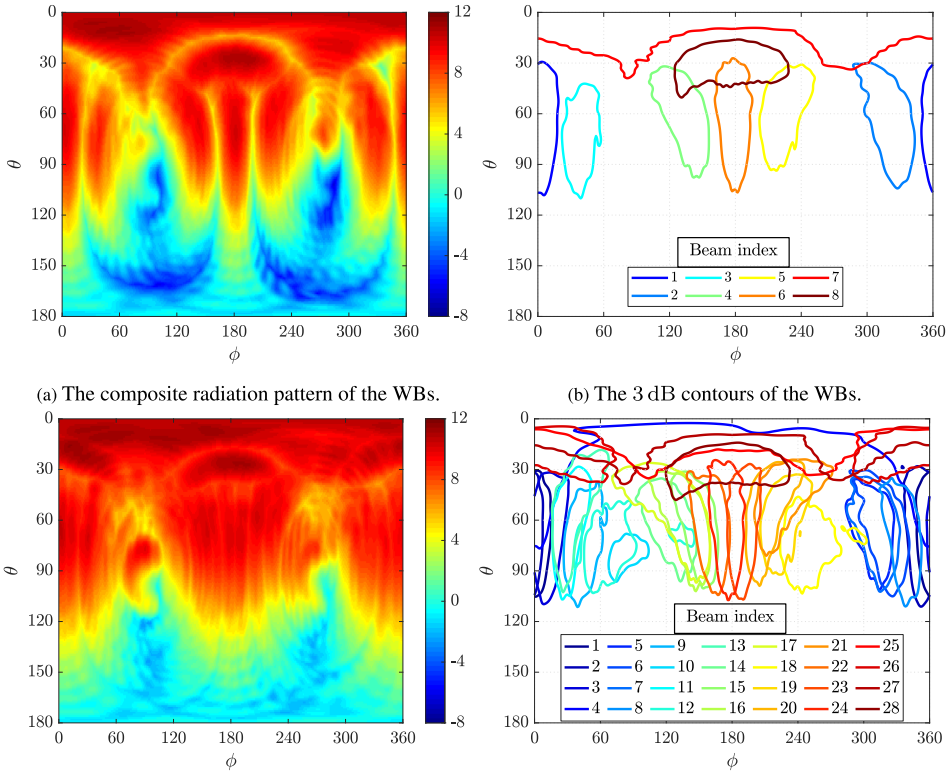

(a) The composite radiation pattern of the WBs.

(b) The 3 dB contours of the WBs.

(c) The composite radiation pattern of the NBs.

(d) The 3 dB contours of the NBs.

FIGURE 8. The composite radiation patterns and the 3 dB contours of the WBs and NB. There are $M_{\text{UE}}^{\text{W}} = 8$ WBs and $M_{\text{UE}}^{\text{N}} = 28$ NBs. The composite radiation pattern is plotted in the dB scale, and the beam indices for the contour plots are given in the legend.

strategy. The communication bandwidth is 100 MHz and subcarrier spacing (SCS) is 240 kHz. The transmit power is $P_{\text{T}} = 30\,30$ dBm. At the UE, we consider that we have codebooks with $M_{\text{UE}}^{\text{W}} = 8$ WBs and $M_{\text{UE}}^{\text{N}} = 28$ NBs. The WB and NB codebooks are obtained using the procedure given in [36]. Both the WBs and NBs cover the whole sphere and are designed assuming 3 bit phase-shifters with no amplitude scaling. The composite radian patterns and the 3 dB contour plots of the beams for the WB and NB codebooks are shown in Fig. 8. The beam decision regions of the same WB and NB codebooks were shown in Fig. 5 and Fig. 6, respectively.

From actual beam measurements, it was observed that even in a static setup, there is substantial variation in the measured RSRP over time. The variation is spatially and temporally correlated. For realistic evaluation, we use the following model to mimic this experimentally observed behavior. Consider that the noise on all M_{UE} receive beams at time t is collected in a vector $\mathbf{n}_t$. To obtain $\mathbf{n}_t$, we consider that the temporal correlation in the noise decreases exponentially, and the parameter η controls the temporal correlation. Let us define a vector $\check{\mathbf{n}}_t \in \mathbb{R}^{M_{\text{UE}} \times 1}$ such that $\check{\mathbf{n}}_t \sim \mathcal{N}(0, \sigma_n^2 \mathbf{I}_{M_{\text{UE}}})$, where σ_n^2 is the noise variance. Further, recall that we need a noise realization every SSB period, i.e., $T_{\text{SS}} = 20$ ms. With this, first, we obtain only temporally correlated noise vector $\bar{\mathbf{n}}_t$

$$\bar{\mathbf{n}}_t = e^{-\eta T_{\text{SS}}} \bar{\mathbf{n}}_{t-1} + \sqrt{1 - e^{-2\eta T_{\text{SS}}}} \check{\mathbf{n}}_t. \tag{15}$$

Further, to introduce correlation across beams, we define a correlation matrix $\mathbf{P} \in \mathbb{R}^{M_{\text{UE}} \times M_{\text{UE}}}$

$$\mathbf{P} = \begin{bmatrix} 1 & \rho & \rho & \cdots & \rho \\ \rho & 1 & \rho & \cdots & \rho \\ \vdots & \vdots & \vdots & \vdots & \\ \rho & \rho & \rho & \cdots & 1 \end{bmatrix}, \tag{16}$$

where $0 \leq \rho \leq 1$ controls the correlation among beams. Specifically, $\rho = 1$ means full correlation and $\rho = 0$ means no correlation. Finally, the spatio-temporally correlated noise vector is $\mathbf{n}_t = \mathbf{P}^{\frac{1}{2}} \bar{\mathbf{n}}_t$, so as to have $\mathbb{E}[\mathbf{n}_t \mathbf{n}_t^*] = \sigma_n^2 \mathbf{P}$. In our experiments, we use $\sigma_n = 4.4$, $\eta = 0.29$, and $\rho = 0.8688$. These parameters are chosen based on measurements done with a mobile phones using a codebook similar to the one used in this paper. Note that, although we generate a $M_{\text{UE}} \times 1$ vector $\mathbf{n}_t$ for each SSB period, only single element of $\mathbf{n}_t$ corresponding to the receive beam j_t is used in the simulation.

3) UE ORIENTATION MODEL AND IMU DETAILS

We consider a filtered random walk based UE orientation model. Specifically, consider a random walk

$$\bar{\alpha}_t = \bar{\alpha}_{t-1} + \mathcal{N}(0, \sigma^2), \tag{17}$$

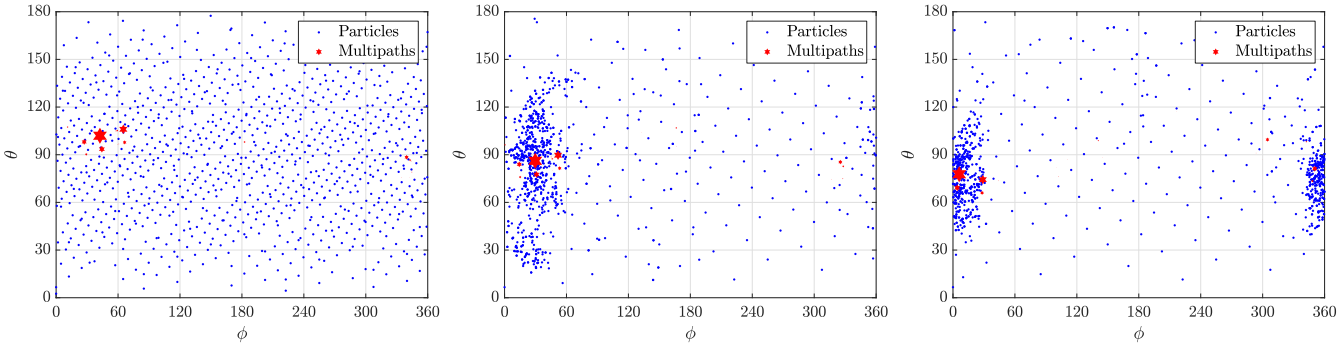

(a) $t = 1$: Initial state of the particles.

(b) $t = 5$: Particles have started to converge around AoA of the strong path.

(c) $t = 9$: Particles converged around AoA of the strong path.

FIGURE 9. Initial convergence of the particles in PF.

where $\bar{\alpha}_0 \sim \mathcal{U}[0°, 360°]$. Then, the filtered random walk is

$$\alpha_t = \frac{1}{K} \sum_{k=0}^{K-1} \bar{\alpha}_{t-k}, \tag{18}$$

where K is the filter length, and larger K implies smoother variation of orientation. The output of the filtered random walk is then wrapped to be within $[0°, 360°]$. We use the same process for obtaining α_t, β_t, and γ_t. In addition, for simplification, we use the same value of σ for generating α_t, β_t, and γ_t. The higher value of σ implies higher rotation. In experiments, we choose the value of σ to be either $1°$ or $10°$. Further, we choose K to be either 5 or 21. It is worthwhile to mention that with $K = 21$, the value $\sigma = 1°$ results in rotation of $8.7°/s$ and $\sigma = 10°$ results in rotation of $87.1°/s$. This level of rotation, however, is around one axis, and as three rotations are applied one after another, the overall rotation can be higher/lower than these values. Note that, the information from IMU sensors is erroneous. The level of error in the sensor measurements can be determined from the sensor specification or from experiments. We model the error as white Gaussian [23]. The error in each axis is parametrized by a value, i.e., σ_α, σ_β, and σ_γ. The values used in our simulation are $\sigma_\alpha = 2°$, $\sigma_\beta = 1°$ and $\sigma_\gamma = 1°$.

4) PF PARAMETER DETAILS

We consider that there are $M = 1000$ particles and the number of uniform particles inserted in each time-step is $N = 150$. These choices were informed by numerical results. Specifically, $M = 1000$ was found to be sufficient to get good performance. Increasing M further increased the computational burden without significantly improving the performance. The value $N = 150$ was obtained by numerically testing the performance of PF for a few values and selecting the one with the best performance. Note that, the error caused by the sensor measurements is only one source of imperfection in the process equation. In practice, the AoA also changes due to the user movement, and the channel changes e.g., multipath fading and channel state change. As these changes are not explicitly modeled in the process equation, they also get implicitly modeled by the process noise. Therefore the optimal level of noise for PF operation is higher than the actual sensor measurement noise, i.e., $\sigma_\alpha = 2°$, $\sigma_\beta = 1°$ and $\sigma_\gamma = 1°$. We did numerical optimization to find that $4\times$ the sensor measurement noise level gives the best results for PF. We use a low variance sampler to implement the importance sampling [37]. The advantage of low variance sampling is that it covers the sample space more systematically.

B. INITIAL CONVERGENCE OF PF AND AVOIDING PARTICLE DEPRIVATION

We first show the convergence of particles to the strongest paths in the channel and the ability of PF to avoid particle deprivation when the channel state changes. In Fig. 9, we show the initial convergence of the PF when the algorithm starts running. Specifically, the AoAs of multipaths in the channel are shown with red stars. The size of the star represents the strength of the multipath. In total, there are $C = 25$ multipaths, but some of them may not be visible in the figure as only a few paths are strong. In Fig. 9a, the initial state of the particles is shown where the particles are uniformly distributed over the sphere. In Fig. 9b, we can see that only after 5 time-steps, the algorithm has started to converge around AoA of the strong path, with good convergence after 9 time-steps as shown in Fig. 9c.

We show the ability of the PF to avoid particle deprivation in Fig. 10. In Fig. 10a, we can see that the PF is successfully tracking the AoAs. Then the channel state changes from NLOS to LOS at time-step 378 as shown in Fig. 10b. This sudden change implies that now the particles correspond to a different spatial region compared to AoA of the strong multipaths. Due to the presence of $N = 150$ uniform particles in every time-step, the PF can recover quickly and the particles converge to the proximity of the AoA of the strong multipaths as shown in Fig. 10c.

C. BENEFIT OF ORIENTATION-ASSISTED BM

We now show the benefit of using orientation information in addition to the RSRP information for BM. For this purpose, we use three metrics. All the metrics are calculated by

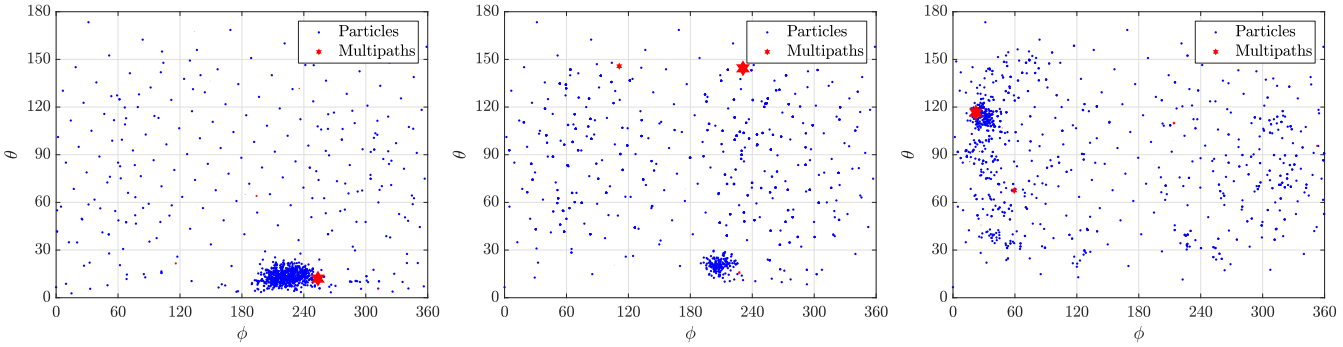

(a) $t = 376$: Particles converged close to the AoA of the strong path.

(b) $t = 378$: Channel state changes from NLOS to LOS with few particles around the new AoA of the strong path.

(c) $t = 390$: Particles have again converged around AoA of the strong path.

FIGURE 10. Change of channel state and subsequent convergence of of the particles in PF.

TABLE 1. The four cases with slow or fast rotation speed, normal or sporadic RSRPs information, and smooth or non-smooth rotation.

Case	Rotation speed (σ)	RSRP information rate (f)	Rotation smoothness (K)
1	Slow (1°)	Normal (1)	Smooth (21)
2	Fast (10°)	Normal (1)	Smooth (21)
3	Fast (10°)	Sporadic (3)	Smooth (21)
4	Fast (10°)	Sporadic (3)	Non-smooth (5)

averaging over the whole UE trajectory. First is the beam prediction accuracy. This metric, simply called "AC" is the percentage of times the beam-predicted by a practical strategy, e.g., "RSRP-only" or "orientation-assisted" is the same as the "genie-aided" best beam. "RSRP-only" is a conventional BM strategy explained at the end of Section II-A, in which RSRP of only one UE beam is updated in one SSB period. The "orientation-assisted" is the proposed PF based strategy. Finally, in the "genie-aided" strategy, the best beam is obtained assuming instantaneous RSRP knowledge of all the beams in the UE codebook. The second metric is the mean RSRP which is simply called "RSRP". The third metric is "RSRP loss" simply called "Loss". This metric is obtained by subtracting the RSRP of the predicted beam of a practical strategy from the RSRP of the genie-aided best beam and taking the mean of the difference. We evaluate these metrics for three UE movement speeds, i.e., $20\,\mathrm{km\,h^{-1}}$, $60\,\mathrm{km\,h^{-1}}$, and $100\,\mathrm{km\,h^{-1}}$. For each UE movement speed we consider a UE with WBs and a UE with NBs. Also, we consider different levels of rotation speed, different RSRP information rates, and different levels of orientation smoothness. Specifically, we create four cases as shown in Table 1. The rotation speed is controlled by σ, i.e., $\sigma = 1°$ implies "Slow" rotation and $\sigma = 10°$ implies "Fast" rotation. The RSRP information rate is controlled by f, i.e., $f = 1$ means a new RSRP measurement every T_{SS} which we call "Normal" information rate, whereas $f = 3$ means a new RSRP measurement every $3T_{\mathrm{SS}}$ which we call "Sporadic" information rate. The rotation smoothness is controlled by K, i.e., $K = 21$ implies "Smooth" rotation, whereas $K = 5$ implies "Non-smooth" rotation. In Table 1, a higher case index implies a more favorable scenario for the use of orientation-information.

The results for this experiment are given in Table 2. From the results of case 1, we can see that the beam prediction accuracy of the orientation-assisted strategy is lower compared to RSRP-only. Similarly mean RSRP is also lower for orientation-assisted strategy, whereas the RSRP loss is higher for orientation-assisted. The reason is that case 1 is not a favorable scenario for the use of orientation information. Specifically, the rotation speed itself is slow so there is not much benefit of using rotation information. In other words, before the mobile significantly rotates, RSRP information on all (or most) beams can be collected to do good BM. Further, as the orientation information is erroneous, using orientation information can harm BM. To an extent, the same observation applies to case 2. Note that, though in the case 2 the rotation is fast, the RSRP information is still collected at a rapid rate, and RSRP information alone is sufficient to do good BM. It is only in the case 3 when the RSRP information rate is lower than the orientation information rate, that the benefit of using the orientation-assisted strategy for BM becomes clear. We can see that depending on the user speed, using the orientation-assisted strategy can improve the beam prediction accuracy by up to 8% and reduce the RSRP loss by up to 2 dB. The benefit of orientation-assisted strategy becomes more pronounced when there is a non-smooth orientation change, i.e., more rapid and sudden orientation change, as in the case 4. Specifically, in this case, the beam prediction accuracy can be improved by up to 10% and RSRP loss can be reduced by up to 2.37 dB. Finally, note that the benefit of the orientation-assisted strategy is clear when RSRP information rate is lower than the orientation information rate. Since it is easy to know RSRP and orientation information rates, the UE can use this information to switch between RSRP-only and orientation-assisted BM. Using this simple switching mechanism, the UE can achieve a performance that is at least as good as RSRP-only in all cases, and in some cases better due to the use of orientation information.

We now give the cumulative distribution function (CDF) of the RSRP of RSRP-only, orientation-assisted, and genie-aided BM strategies. This result is for case 4 with the UE

TABLE 2. The performance comparison of orientation-assisted BM strategy in comparison with RSRP-only BM in terms of beam prediction accuracy (%), mean RSRP (dBm), and RSRP loss (dB). The performance is compared for three different UE movement speeds and four cases outlined in Table 1.

Case			1			2			3			4		
Metric			AC	RSRP	Loss	AC	RSRP	Loss	AC	RSRP	Loss	AC	RSRP	Loss
20 km h^{-1}	WB	RSRP-only	90.16	−101.9	0.17	75.60	−102.57	0.83	49.10	−104.91	3.17	40.43	−105.9	4.15
		Orientation-assisted	73.42	−102.57	0.84	70.65	−102.84	1.10	54.80	−104.53	2.78	50.58	−104.97	3.22
	NB	RSRP-only	63.49	−100.98	0.86	28.55	−104.51	4.42	13.11	−107.63	7.54	11.14	−108.04	7.94
		Orientation-assisted	37.14	−102.99	2.87	33.05	−103.38	3.29	21.72	−105.56	5.47	21.41	−105.66	5.57
60 km h^{-1}	WB	RSRP-only	85.36	−102.59	0.41	72.20	−103.06	1.09	44.16	−105.65	3.68	36.87	−106.53	4.56
		Orientation-assisted	69.06	−103.36	1.18	67.83	−103.3	1.33	49.75	−105.28	3.31	47.19	−105.56	3.60
	NB	RSRP-only	53.39	−102.21	1.76	26.36	−105.1	4.84	10.74	−108.33	8.07	9.53	−108.73	8.43
		Orientation-assisted	31.62	−103.93	3.48	30.31	−103.95	3.69	18.73	−106.46	6.20	18.34	−106.5	6.20
100 km h^{-1}	WB	RSRP-only	81.07	−102.43	0.66	69.31	−103.22	1.30	41.12	−106.03	4.11	34.52	−106.78	4.86
		Orientation-assisted	67.46	−103.12	1.35	65.03	−103.52	1.60	45.29	−105.76	3.84	42.98	−106.02	4.10
	NB	RSRP-only	46.73	−102.66	2.47	23.86	−105.6	5.26	9.88	−108.52	8.17	9.45	−108.86	8.48
		Orientation-assisted	29.24	−104.28	4.09	27.79	−104.64	4.30	17.00	−106.97	6.63	15.98	−107.14	6.76

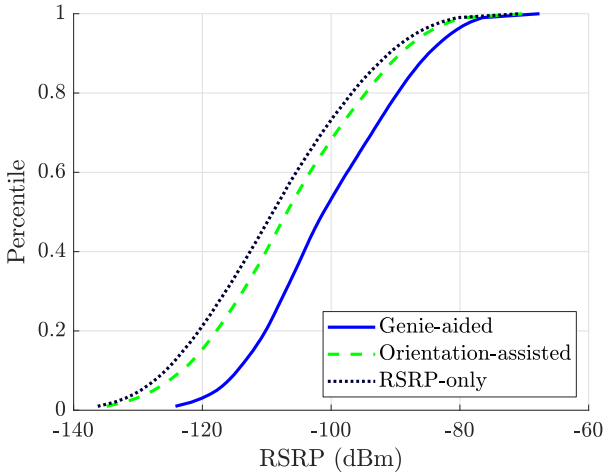

FIGURE 11. RSRP CDF comparison of genie-aided, RSRP-only and orientation-assisted BM. The orientation-assisted BM does better than RSRP-only due to the use of orientation information.

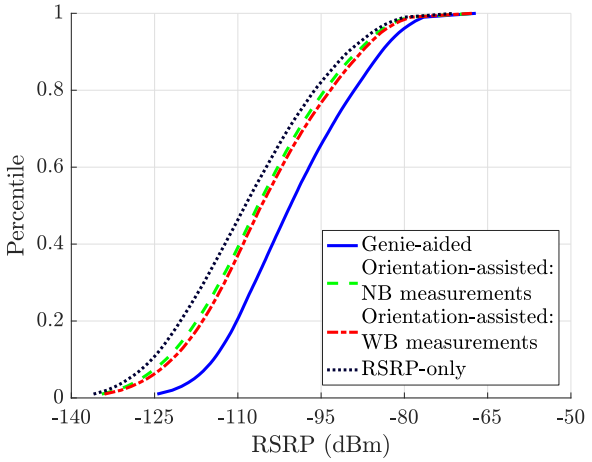

FIGURE 12. RSRP CDF comparison of of genie-aided, RSRP-only and orientation-assisted strategies, with results collected over the whole 20 km trajectory. The WB RSRPs based orientation-assisted strategy does slightly better than NB RSRPs based orientation-assisted strategy.

speed of 60 km h^{-1} and NBs. From the results in Fig. 11 we can see that the benefit of using the orientation-assisted strategy is not limited to a specific percentile region, but the CDF of orientation-assisted strategy is better than RSRP-only in all percentile regions.

D. PREDICTING NBS FROM WB RSRPS

Finally, we give a result for predicting NBs using WB RSRPs in Fig. 12. The result is for case 4 with the UE speed of 60 km h^{-1}. For orientation-assisted strategies, there are two curves. First is "orientation-assisted: NB measurements" which corresponds to the case of using NB RSRPs for predicting NBs. The second is "orientation-assisted: WB measurements" which corresponds to the case of using WB RSRPs for predicting NBs. We can see from the results that the WB RSRPs based strategy has superior performance compared to the NB RSRPs. The advantage, however, is not significant. Specifically, the median gain by using WB measurements over NB measurements is 0.64 dB. This is because the benefit of using WB measurements over NB measurements is pronounced only when the channel state changes or for

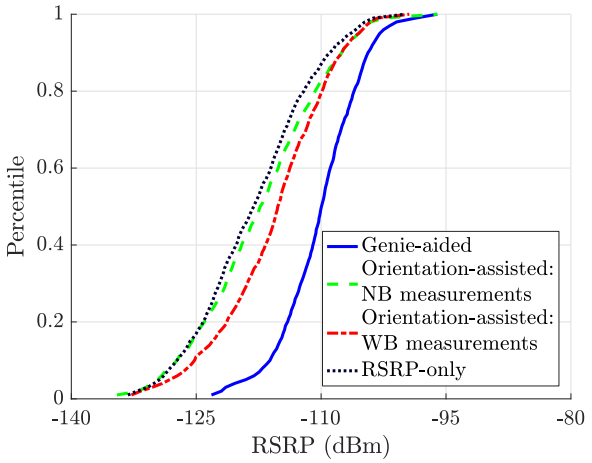

FIGURE 13. RSRP CDF comparison of of genie-aided, RSRP-only and orientation-assisted strategies, with results collected over the initial 84 time-steps. The WB RSRPs based orientation-assisted strategy does significantly better than NB RSRPs based orientation-assisted strategy.

initial convergence. The results presented in Fig. 12, however, are collected over the whole 20 km trajectory. As there are a handful of channel state changes over the trajectory, the

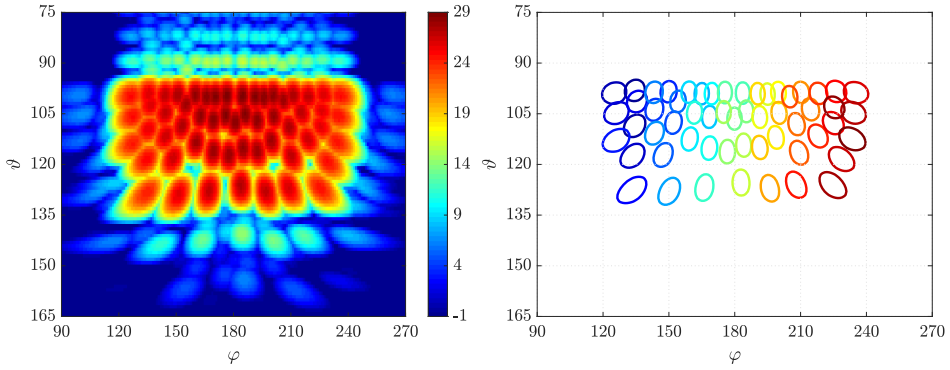

(a) The composite radiation pattern of the BS codebook.

(b) The 3 dB contours of the BS beams.

FIGURE 14. **The composite radiation pattern (in dB scale) and the 3 dB contours of the beams in BS codebook. There are $M_{\text{BS}} = 56$ beams, and the codebook is designed to serve the ground UEs (hence vertical coverage for $\vartheta > 90°$) and covers one 120° sector (hence horizontal coverage for $\varphi \in [120°, 240°]$).**

advantage of using WB measurements is not clear. In Fig. 13, we compare the CDFs for initial few time-steps. Specifically, we show the results for initial $M_{\text{UE}}^{\text{N}} \times f$, i.e., $28 \times 3 = 84$ time-steps. Note that, in 84 time-steps one cycle of NB measurements is completed when a new RSRP is available every 3 T_{SS}. We can see from Fig. 13 that the benefit of using WB measurements is more pronounced in the initial time-steps. Specifically, the median gain by using WB measurements over NB measurements is 2.1 dB in this case.

E. MULTI-ANTENNA BS

So far we have assumed a single isotropic antenna at the BS. We now consider a 16 × 16 uniform planar array (UPA) at the BS, and a beam codebook containing $M_{\text{BS}} = 56$ beams. The composite radiation pattern and the 3 dB contours of the beams in BS codebook are shown in Fig. 14. The codebook is designed assuming 5 bit phase-shifters with no amplitude scaling. Further, the codebook is designed to serve the ground UEs and hence the vertical coverage is for $\vartheta > 90°$. The codebook covers one 120° sector horizontally and hence horizontal coverage is for $\varphi \in [120°, 240°]$ ($\varphi = 180°$ points to the positive x axis in Fig. 7). We assume genie-aided knowledge of the best transmit beam, i.e., the BS beam that yields the highest RSRP value for any UE beam. With the knowledge of the BS beam, the problem of finding a UE beam is the same as what we have considered so far. For brevity, we only show the results for the case 4, with NBs at the UE, and the movement speed of 20 km h^{-1}. Note that this is the case that had yielded a gain of 2.37 dB with isotropic BS (see Table 2). The CDF for this experiment is shown in Fig. 15. The mean RSRP gain by using the proposed orientation-assisted strategy in comparison with RSRP-only is now 3.84 dB. This is 1.47 dB better than the 2.37 dB which was achieved with an isotropic BS. Similarly, the beam prediction accuracy by using the proposed orientation-assisted approach is now 15.5% higher than the RSRP-only, in comparison with 10% with an isotropic BS. This improved performance

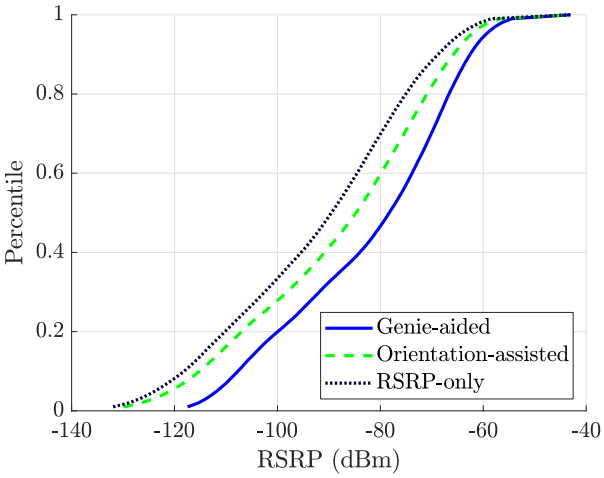

FIGURE 15. **RSRP CDF comparison of of genie-aided, RSRP-only and orientation-assisted strategies, with $M_{\text{BS}} = 56$ beams. The proposed orientation-assisted strategy does better than the RSRP-only strategy in all percentile ranges.**

is a result of channel sparsification by the use of BS beams and verifies the intuition that using isotropic BS is a pessimistic setup for the proposed strategy.

VI. CONCLUSION AND FUTURE WORK

We proposed a beam management (BM) strategy based on fusing reference signal received power (RSRP) and orientation information using particle filter (PF). Specifically, we formulated the BM problem as an angle-of-arrival (AoA) tracking problem followed by beam determination by counting the number of particles in the beam decision regions of the beams. The proposed strategy improves over RSRP-only BM, particularly in cases that are favorable for using orientation information i.e., when the rotation is high and non-smooth and the RSRP information is available sporadically. Using the proposed orientation-assisted strategy, the BM accuracy can be improved by 15.5% and the RSRP loss can be reduced

by 3.84 dB. The RSRP improvement of 3.84 dB (equivalent to 59% transmission power reduction) at the UE is substantial and can considerably improve the battery life.

For future work, note that the proposed strategy has been evaluated with practical assumptions, i.e., realistic ray-tracing channels, user equipment (UE) and base station (BS) codebooks, RSRP noise, and inertial measurement unit (IMU) noise. The proposed strategy, however, needs to be implemented and evaluated on a mobile device. This includes computational complexity analysis and optimization (e.g., by using appropriate resampling strategies, e.g., [38] and/or by using augmented PF [37]) when implemented on the UE. Further, in this work, we considered analog beamforming based on phase-shifters. Extending the proposed strategy for hybrid analog-digital architectures, where multiple RSRPs can be available at the same time is also an interesting direction. Finally, equipped with the AoA estimate, the UE does not need to sweep the beams in a round-robin manner, which is inefficient during the beam tracking stage. Instead, the UE can choose to sweep the predicted best beam (and the neighboring beams of the predicted best beam). The design and evaluation of this strategy are left for future work.

REFERENCES

[1] Z. Pi and F. Khan, "An introduction to millimeter-wave mobile broadband systems," *IEEE Commun. Mag.*, vol. 49, no. 6, pp. 101–107, Jun. 2011.

[2] T. S. Rappaport, S. Sun, R. Mayzus, H. Zhao, Y. Azar, K. Wang, G. N. Wong, J. K. Schulz, M. Samimi, and F. Gutierrez, "Millimeter wave mobile communications for 5G cellular: It will work!," *IEEE Access*, vol. 1, pp. 335–349, May 2013.

[3] M. Giordani, M. Polese, M. Mezzavilla, S. Rangan, and M. Zorzi, "Toward 6G networks: Use cases and technologies," *IEEE Commun. Mag.*, vol. 58, no. 3, pp. 55–61, Mar. 2020.

[4] M. Giordani, M. Polese, A. Roy, D. Castor, and M. Zorzi, "A tutorial on beam management for 3GPP NR at mmWave frequencies," *IEEE Commun. Surveys Tuts.*, vol. 21, no. 1, pp. 173–196, 1st Quart., 2019.

[5] N. Garcia, H. Wymeersch, E. G. Strom, and D. Slock, "Location-aided mm-wave channel estimation for vehicular communication," in *Proc. IEEE Int. Workshop Signal Process. Adv. Wireless Commun. (SPAWC)*, Jul. 2016, pp. 1–5.

[6] V. Va, T. Shimizu, G. Bansal, and R. W. Heath, Jr., "Position-aided millimeter wave V2I beam alignment: A learning-to-rank approach," in *Proc. IEEE 28th Annu. Int. Symp. Pers., Indoor, Mobile Radio Commun. (PIMRC)*, Oct. 2017, pp. 1–5.

[7] A. Ali, N. González-Prelcic, and R. W. Heath, Jr., "Millimeter wave beam-selection using out-of-band spatial information," *IEEE Trans. Wireless Commun.*, vol. 17, no. 2, pp. 1038–1052, Feb. 2018.

[8] A. Ali, N. González-Prelcic, and R. W. Heath, Jr., "Spatial covariance estimation for millimeter wave hybrid systems using out-of-band information," *IEEE Trans. Wireless Commun.*, vol. 18, no. 12, pp. 5471–5485, Dec. 2019.

[9] A. Klautau, N. González-Prelcic, and R. W. Heath, Jr., "LIDAR data for deep learning-based mmWave beam-selection," *IEEE Wireless Commun. Lett.*, vol. 8, no. 3, pp. 909–912, Jun. 2019.

[10] A. Ali, N. González-Prelcic, and A. Ghosh, "Millimeter wave V2I beam-training using base-station mounted radar," in *Proc. IEEE Radar Conf.*, Apr. 2019, pp. 1–5.

[11] A. Ali, N. González-Prelcic, and A. Ghosh, "Passive radar at the roadside unit to configure millimeter wave vehicle-to-infrastructure links," *IEEE Trans. Veh. Technol.*, vol. 69, no. 12, pp. 14903–14917, Dec. 2020.

[12] M. Alrabeiah, A. Hredzak, and A. Alkhateeb, "Millimeter wave base stations with cameras: Vision-aided beam and blockage prediction," in *Proc. IEEE Veh. Technol. Conf. (VTC-Spring)*, May 2020, pp. 1–5.

[13] G. Charan, M. Alrabeiah, and A. Alkhateeb, "Vision-aided dynamic blockage prediction for 6G wireless communication networks," 2020, *arXiv:2006.09902*. [Online]. Available: http://arxiv.org/abs/2006.09902

[14] A. Alammouri, J. Mo, B. L. Ng, J. C. Zhang, and J. G. Andrews, "Hand grip impact on 5G mmWave mobile devices," *IEEE Access*, vol. 7, pp. 60532–60544, 2019.

[15] Y. Wang, A. Klautau, M. Ribero, A. C. K. Soong, and R. W. Heath, Jr., "MmWave vehicular beam selection with situational awareness using machine learning," *IEEE Access*, vol. 7, pp. 87479–87493, 2019.

[16] W. Xu, F. Gao, S. Jin, and A. Alkhateeb, "3D scene-based beam selection for mmWave communications," *IEEE Wireless Commun. Lett.*, vol. 9, no. 11, pp. 1850–1854, Nov. 2020.

[17] D.-S. Shim, C.-K. Yang, J. Kim, J. Han, and Y. Cho, "Application of motion sensors for beam-tracking of mobile stations in mmWave communication systems," *Sensors*, vol. 14, no. 10, pp. 19622–19638, Oct. 2014.

[18] Z. Qi and W. Liu, "Three-dimensional millimetre-wave beam tracking based on smart phone sensor measurements and direction of arrival/time of arrival estimation for 5G networks," *IET Microw., Antennas Propag.*, vol. 12, no. 3, pp. 271–279, Feb. 2018.

[19] M. Brambilla, M. Nicoli, S. Savaresi, and U. Spagnolini, "Inertial sensor aided mmWave beam tracking to support cooperative autonomous driving," in *Proc. IEEE Int. Conf. Commun. Workshops (ICC Workshops)*, May 2019, pp. 1–6.

[20] S. Rezaie, C. N. Manchón, and E. de Carvalho, "Location- and orientation-aided millimeter wave beam selection using deep learning," in *Proc. IEEE Int. Conf. Commun. (ICC)*, Jun. 2020, pp. 1–6.

[21] V. Va, H. Vikalo, and R. W. Heath, Jr., "Beam tracking for mobile millimeter wave communication systems," in *Proc. IEEE Global Conf. Signal Inf. Process. (GlobalSIP)*, Dec. 2016, pp. 743–747.

[22] S. Jayaprakasam, X. Ma, J. W. Choi, and S. Kim, "Robust beam-tracking for mmWave mobile communications," *IEEE Commun. Lett.*, vol. 21, no. 12, pp. 2654–2657, Dec. 2017.

[23] M. Kok, J. D. Hol, and T. B. Schön, "Using inertial sensors for position and orientation estimation," *Found. Trends Signal Process.*, vol. 11, nos. 1–2, pp. 1–153, 2017.

[24] *Study on Channel Model for Frequencies From 0.5 to 100 GHz*, document TR 38.901, 3GPP, Version 14.3.0, Dec. 2017. [Online]. Available: http://www.3gpp.org/DynaReport/38901.htm

[25] N. J. Gordon, D. J. Salmond, and A. F. M. Smith, "Novel approach to nonlinear/non-Gaussian Bayesian state estimation," *IEE Proc. F, Radar Signal Process.*, vol. 140, no. 2, pp. 107–113, Apr. 1993.

[26] A. Doucet, S. Godsill, and C. Andrieu, "On sequential Monte Carlo sampling methods for Bayesian filtering," *Statist. Comput.*, vol. 10, no. 3, pp. 197–208, Jul. 2000.

[27] M. S. Arulampalam, S. Maskell, N. Gordon, and T. Clapp, "A tutorial on particle filters for online nonlinear/non-Gaussian Bayesian tracking," *IEEE Trans. Signal Process.*, vol. 50, no. 2, pp. 174–188, Feb. 2002.

[28] R. Swinbank and R. J. Purser, "Fibonacci grids: A novel approach to global modelling," *Quart. J. Roy. Meteorol. Soc.*, vol. 132, no. 619, pp. 1769–1793, Jul. 2006.

[29] M. Dehghani Soltani, A. A. Purwita, Z. Zeng, C. Chen, H. Haas, and M. Safari, "An orientation-based random waypoint model for user mobility in wireless networks," in *Proc. IEEE Int. Conf. Commun. Workshops (ICC Workshops)*, Jun. 2020, pp. 1–6.

[30] M. D. Soltani, M. A. Arfaoui, I. Tavakkolnia, A. Ghrayeb, M. Safari, C. M. Assi, M. O. Hasna, and H. Haas, "Bidirectional optical spatial modulation for mobile users: Toward a practical design for LiFi systems," *IEEE J. Sel. Areas Commun.*, vol. 37, no. 9, pp. 2069–2086, Sep. 2019.

[31] M. D. Soltani, A. A. Purwita, Z. Zeng, H. Haas, and M. Safari, "Modeling the random orientation of mobile devices: Measurement, analysis and LiFi use case," *IEEE Trans. Commun.*, vol. 67, no. 3, pp. 2157–2172, Mar. 2019.

[32] A. A. Purwita, M. D. Soltani, M. Safari, and H. Haas, "Terminal orientation in OFDM-based LiFi systems," *IEEE Trans. Wireless Commun.*, vol. 18, no. 8, pp. 4003–4016, Aug. 2019.

[33] B. H. Fleury, "First- and second-order characterization of direction dispersion and space selectivity in the radio channel," *IEEE Trans. Inf. Theory*, vol. 46, no. 6, pp. 2027–2044, Sep. 2000.

[34] *Wireless Insite*. Accessed: Feb. 12, 2021. [Online]. Available: http://www.remcom.com/wireless-insite

[35] P. Hart, N. Nilsson, and B. Raphael, "A formal basis for the heuristic determination of minimum cost paths," *IEEE Trans. Syst. Sci. Cybern.*, vol. SSC-4, no. 2, pp. 100–107, Jul. 1968.

[36] J. Mo, B. L. Ng, S. Chang, P. Huang, M. N. Kulkarni, A. Alammouri, J. C. Zhang, J. Lee, and W.-J. Choi, "Beam codebook design for 5G mmWave terminals," *IEEE Access*, vol. 7, pp. 98387–98404, 2019.

[37] S. Thrun, W. Burgard, and D. Fox, *Probabilistic Robotics*. Cambridge, MA, USA: MIT Press, 2005.
[38] M. A. Nicely and B. E. Wells, "Improved parallel resampling methods for particle filtering," *IEEE Access*, vol. 7, pp. 47593–47604, 2019.

ANUM ALI (Member, IEEE) received the B.S. degree from COMSATS University Islamabad (CUI), Islamabad, Pakistan, in 2011, the M.S. degree from the King Fahd University of Petroleum and Minerals, Dhahran, Saudi Arabia, in 2014, and the Ph.D. degree from The University of Texas at Austin, Austin, TX, USA, in 2019, all in electrical engineering. From 2011 to 2012 and from 2014 to 2015, he held research positions at CUI and the King Abdullah University of Science and Technology, Thuwal, Saudi Arabia, respectively. He held visiting positions at the California Institute of Technology, Pasadena, CA, USA, in 2015, and Aalborg University, Aalborg, Denmark, in 2017. In 2016, 2017, and 2018, he held internship positions at Intel Corporation, Santa Clara, CA, USA, Qualcomm, Bridgewater, NJ, USA, and Nokia Bell Labs, Naperville, IL, USA. He is currently a Senior Engineer with Samsung Research America, Plano, TX, USA. His research interest includes the applications of signal processing in wireless communications.

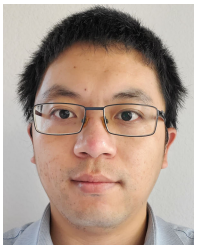

JIANHUA MO (Member, IEEE) received the B.S. and M.S. degrees from Shanghai Jiao Tong University, in 2010 and 2013, respectively, and the Ph.D. degree from The University of Texas at Austin, in 2017, all in electrical engineering.

He is currently a Staff Engineer with Samsung Research America, Plano, TX, USA. His research interests include physical layer security, and MIMO communications with low resolution ADCs. He is also involved in the development of mmWave wireless backhaul transmission and 5G UE beam codebook. His awards and honors include the Heinrich Hertz Award for Best Communications Letter in 2013, the Exemplary Reviewer of the IEEE Wireless Communications Letters in 2012 and the IEEE Communications Letters in 2015, and a Finalist for Qualcomm Innovation Fellowship in 2014.

BOON LOONG NG (Member, IEEE) received the B.Eng. degree in electrical and electronic engineering and the Ph.D. degree in engineering from The University of Melbourne, Australia, in 2001 and 2007, respectively.

He currently holds the position of a Research Director with the Standards and Mobility Innovation (SMI) Laboratory, Samsung Research America, Plano, TX, USA. He had contributed to 3GPP RAN L1/L2 standardizations of LTE, LTE-A, LTE-A Pro, and 5G NR technologies from the period of 2008 to 2018. He holds over 60 USPTO-granted patents on LTE/LTE-A/LTE-A Pro/5G and more than 100 patent applications globally. Since 2018, he has been leading a Research and Development team that develops system and algorithm design solutions for commercial 5G and Wi-Fi technologies.

VUTHA VA (Member, IEEE) received the B.E. and M.E. degrees in electrical and electronic engineering from the Tokyo Institute of Technology, in 2011 and 2013, respectively, and the Ph.D. degree in electrical and computer engineering from The University of Texas at Austin, in 2018. He is currently a Staff Engineer with the Standards and Mobility Innovation Laboratory, Samsung Research America. His research interests include vehicular communications, millimeter wave communications, the fifth generation (5G) cellular networks, millimeter wave radar, and machine learning.

JIANZHONG CHARLIE ZHANG (Fellow, IEEE) received the Ph.D. degree from the University of Wisconsin, Madison. He is currently a SVP and the Head of the Standards and Mobility Innovation Laboratory, Samsung Research America, where he leads research, prototyping, and standards for 5G and future multimedia networks. From 2009 to 2013, he has served as the Vice Chairman for the 3GPP RAN1 working group and led development of LTE and LTE-Advanced technologies, such as 3D channel modeling, UL-MIMO, CoMP, and Carrier Aggregation for TD-LTE.